Sensors and Actuators B 226 (2016) 156–169

Contents lists available at ScienceDirect

Sensors and Actuators B: Chemical

journal homepage: www.elsevier.com/locate/snb

Selective detection of part per billion concentrations of ammonia using a p–n semiconducting oxide heterostructure

Chenhu Sun, Prabir K. Dutta*

Department of Chemistry and Biochemistry, The Ohio State University, Columbus, OH 43210, United States

ARTICLE INFO

Article history:
Received 24 July 2015
Received in revised form 3 November 2015
Accepted 19 November 2015
Available online 23 November 2015

Keywords:
Interference
Breath analysis
Nickel oxide
Indium oxide
Infrared spectroscopy
Sensing mechanism

ABSTRACT

Detection of low levels of ammonia is relevant for environmental, combustion and health-related applications. Resistive semiconducting metal oxide sensing platforms are extensively studied for ammonia and other gas detection. Two important aspects of gas sensing are enhancing sensitivity and selectivity. In this paper, we present a sensor platform with n-type In_2O_3 and p-type NiO placed side by side with a shared 30 μm interface. The substrate on which these metal oxides are placed allows for measuring the resistance change across In_2O_3, NiO or any combination of both oxides. Our focus was to develop an ammonia sensor with ppb sensitivity, with possible application in breath analysis. With low concentrations of NH_3 (<100 ppb), the change in resistance with NiO was anomalous at 300 °C, the resistance decreased and then gradually increased over tens of minutes before decreasing again to reach the baseline. In situ diffuse reflectance infrared spectroscopy exhibited a band at 1267 cm^{-1}, which was assigned to O_2^- and the change in intensity of this band with time mirrored the transient change in resistance with 1 ppm NH_3 at 300 °C, indicating that NH_3 chemisorption was correlated with the O_2^- species. Taking advantage of the transient resistance decrease of NiO with NH_3, and combining the In_2O_3 and NiO allowed selectivity enhancement towards NH_3 at concentrations as low as 100 ppb. Interference to CO, NO_x and humidity were studied. By selecting a suitable combination of both oxides, the response to CO at <10 ppm could be negated. Similarly, with NO at <10 ppb, there was minimal sensor response. The sensor was used to analyze NH_3 mixed into human breath at 10–1000 ppb concentrations. Water had to be completely removed from the breath via a moisture trap, since water interfered with the NH_3 chemisorption chemistry. Potential applications of this sensor platform in breath analysis are discussed.

1. Introduction

Methods for measurement of ammonia (NH_3) are relevant to environmental, combustion and health related industries [1]. Ammonia in atmosphere arises primarily from anthropogenic sources, including agriculture (nitrogen fixation, ammonification) and emissions from chemical industry involved in development of refrigeration and fertilizers. Ammonia is a lachrymatory gas, and breathing ammonia at high concentrations (~1000 ppm) can induce laryngospasms, and cause bronchiectasis [2,3], and thus need for environmental ammonia monitors. The transportation industry is interested in measuring ammonia from exhaust emissions, air quality control in passenger compartment and in a new generation of lean-burn combustion engines, where the exhaust gas after-treatment includes reaction of nitrogen oxides with ammonia. Ammonia is also produced in the human body and the health industry is interested in monitoring ammonia in exhaled human breath for disease diagnosis. In particular, breath ammonia measurement has the potential to probe several diseases including malfunctioning of liver and kidney [4], *H. pylori* infection [5] and halitosis [6]. The concentration ranges over which ammonia detection is relevant for these applications range from 0.1 ppm (health) to hundreds of ppm (environmental).

Different measurement principles have been applied for the detection of ammonia, including optical spectroscopy, electrochemistry and wet-chemistry methods. A particularly challenging application is the detection of ammonia in human breath. [7]. Tunable diode laser absorption spectroscopy has been used to detect ammonia in breath, with detection limit of 1 ppm [8]. A quantum cascade laser diode was able to measure ammonia as low as 4 ppb [9]. Other strategies include use of quartz crystal microbalance [10] and liquid-film conductive sensor [11]. Sensors based on

* Corresponding author.
E-mail address: dutta.1@osu.edu (P.K. Dutta).

http://dx.doi.org/10.1016/j.snb.2015.11.085
0925-4005/

conducting polymer junctions can detect ppb ammonia in human breath [12–15], and a p-n heterojunction polyaniline–TiO_2 sensor is reported to have ppt sensitivity [16]. Mass spectrometry also can measure ammonia down to ppb levels [17]. Instruments for measuring ammonia are often bulky [18], and there is a drive for obtaining miniaturized sensors.

Solid state electrochemical sensors have been developed for monitoring ammonia. This technology is attractive since high sensitivity, selectivity, and fast response time are possible. In addition, these devices have advantages of low power consumption, light-weight, low maintenance cost, harsh environment tolerance and portability. There are numerous papers on resistive semiconducting metal oxide sensors for ammonia. The working principle of these devices is associated with the adsorption of gas molecules on the oxide's surface inducing charge transfer, which result in changes in resistance of the oxide. Semiconducting metal oxides such as n-type WO_3 [19–21], SnO_2 [22,23], In_2O_3 [24,25], ZnO [26,27], TiO_2 [28], MoO_3 [29] as well as p-type Cr_2O_3 [30], NiO [31], CuO [32], have been studied as sensing materials to detect NH_3. To promote sensitivity and selectivity, noble metals like Pt [33], Pd [34], Au [35] and Ag [36] have been introduced to metal oxides. Of these, MoO_3-based sensors have been developed for measuring ammonia in human breath [29,37].

However, developing an electrochemical sensor platform that can measure low concentrations of ammonia in the environment, in optimizing combustion processes and in human breath is still a challenge. There is the need for ppb sensitivity, discrimination against other gases present at much higher concentrations, and in the case of combustion, the ability to tolerate harsh environments, and be insensitive to other exhaust gases.

Mixtures of p- and n-semiconducting oxides can improve sensor performance. Examples include anatase/rutile for CO detection, ZnO/NiO for NH_3 detection, In_2O_3/NiO for ethanol detection, and CuO/SnO_2 for H_2S detection [38–41]. These designs are mixtures of p- and n-powders, or the p-type material grown on n-type powders and vice versa. In addition, isotype heterojunctions, prepared by mixing powders, such as WO_3 and ZnO have also shown selective gas sensing [42].

We recently reported a different way of combining p- and n-type semiconducting oxides, and demonstrated sensing of nitric oxide gas in ppb levels [43]. In this paper, we explore a similar design for sensing ammonia. The sensor device comprises adjacent alignment of p-type NiO and n-type In_2O_3 deposited on a gold microspring array. We demonstrate detection of ammonia at ppb levels, while discriminating against nitric oxide at ppb levels, and carbon monoxide at significantly higher ppm concentrations using this semiconductor hetero-junction structure. A potential application of detection of ammonia in human breath samples is also demonstrated, suggesting the application of this sensor platform in a future breath monitoring device.

2. Experimental

2.1. Chemicals and materials

Indium (II) oxide (99.99%, metals basis, ~325 mesh powder), nickel (II) oxide (99.998%, metals basis), alpha-terpineol (96%), gold wires (0.127 mm dia, 99.99%) were purchased from Alfa Aesar (Ward Hill, USA). The plastic substrates with gold microspring arrays were obtained from FormFactor, Inc. (USA). The interdigitated electrodes were obtained from Case Western Reserve University. All test gases including nitrogen, oxygen, ammonia and carbon monoxide were supplied by Praxair (Danbury, USA).

2.2. Sensor fabrication

The procedures of sensor fabrication are shown in Figs. 3 and 4. The plastic substrate was washed by ethanol and distilled water. Gold wires were connected with the gold micro springs on the substrate. The commercial powders were ground thoroughly before use. 1 g of NiO powder was dispersed in 0.4 mL terpineol and blended into a thick slurry. 80 mg of the obtained NiO slurry was evenly painted onto the left side of the substrate. Then 1 g of In_2O_3 powder was mixed with 0.4 mL terpineol and 20 mg of the slurry was painted onto the right side of the substrate with a common interface. According to the area divided by vertical lines of four gold microsprings, the as-fabricated area ratio of the two semiconductors turned out to be 14:4 on the surface of the substrate (17.5 mm × 4.5 mm). The substrate was designed in such a fashion that it has several leads at different distances, so that resistance across different lengths of the oxides could be measured. The sensor was calcined in air at 320 °C for 2 h and kept in a tube furnace at 300 °C with flowing 20% O_2 in N_2 overnight before testing. The polymer substrate decomposed at 350 °C, so alumina substrates of 10 mm × 10 mm with interdigitated gold lines of 0.25 mm spacing were used for high temperature measurements. After calcination at 320 °C in air for 2 h, the semiconductor layer was typically about 200 μm thick (discussed later).

2.3. Characterization

The phase and crystallinity of the metal oxides were analyzed by a Bruker D8 Advance X-ray diffractometer. The surface morphology of the sensor was investigated by a Quanta 200 scanning electron microscope. The chemical state of the metal oxides was examined by a Kratos X-ray photoelectron spectrometer with a mono Al source. The current-voltage measurement was performed on a CHI760D electrochemical workstation. The gas–solid interactions were studied by a PerkinElmer Spectrum 400 FTIR spectrometer coupled with a diffuse reflectance accessory. The Raman mapping of the interface was performed on a Renishaw - Smiths Raman Microprobe.

2.4. Gas sensing measurements

All gas sensing experiments were performed within a quartz tube placed inside a tube furnace (Lindberg/Blue) at 300 °C, with a PC-controlled gas delivery system with calibrated mass flow controllers (Sierra Instruments INC.). The test gas mixtures containing different concentrations of NH_3 at constant oxygen content of 20 vol% were prepared by diluting NH_3 with O_2 and N_2. The total flow rate was maintained at 200 cm^3/min. The resistance of the sensor was recorded by an Agilent 34972A LXI data acquisition/switch unit at a scan rate of 0.1 Hz.

2.5. Human breath sensing measurements

A system that simulates human breath with trace ammonia gas was developed. The system comprises a Mylar bag containing exhaled human breath samples and an ammonia gas cylinder. The trace ammonia gas at physiologically relevant concentrations was determined by controlling the flow rates of breath samples from the Mylar bags and ammonia supply, respectively. The total flow rate was maintained at 200 cm^3/min. Three setups were designed. A first setup used a 37 °C water vapor bath to keep a constant humidity in the mixture of NH_3 and breath sample. The second setup used a dry ice/acetonitrile bath maintained at −20 to −25 °C to completely remove humidity in the mixture of breath + NH_3 and also an ice bath to reduce humidity. In both these setups, the breath sample was used as the background and NH_3 was spiked into the

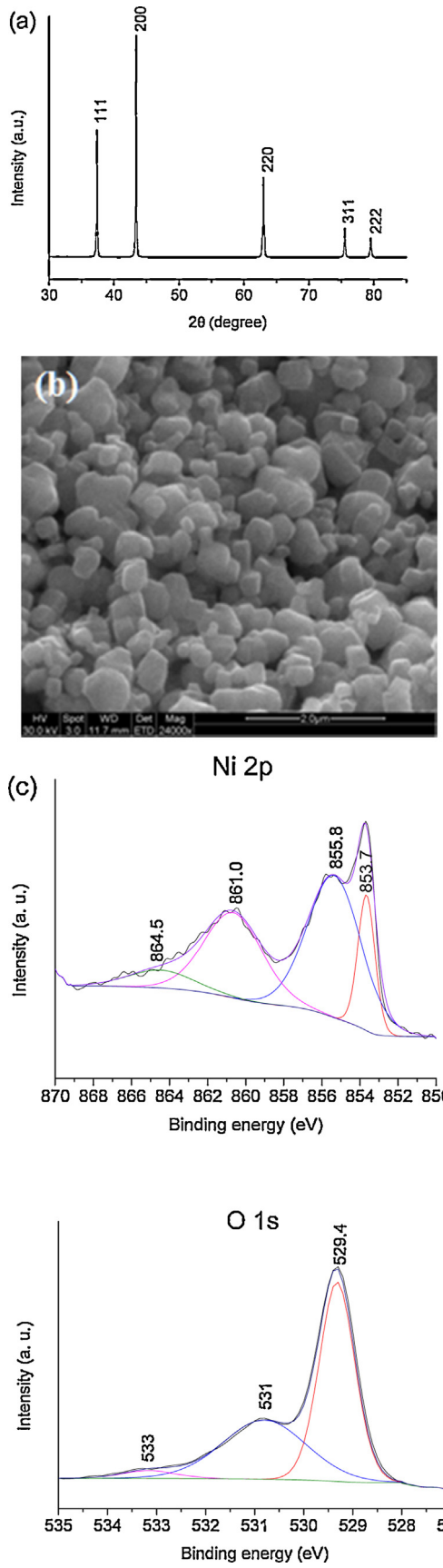

Fig. 1. (a) XRD patterns of NiO powder annealed at 320 °C; (b) SEM image of NiO film on the sensor; (c) XPS spectra of the Ni 2p and O 1s region for NiO powder annealed at 320 °C.

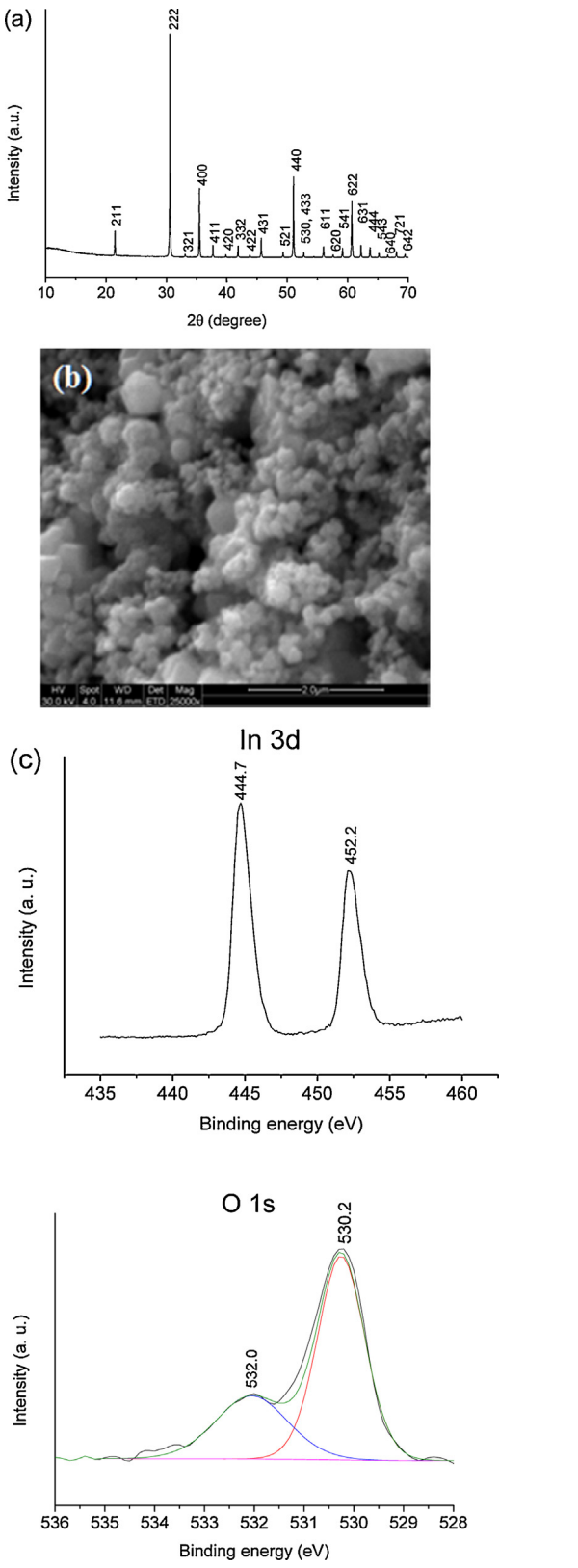

Fig. 2. (a) XRD patterns of In_2O_3 powder annealed at 320 °C; (b) SEM image of In_2O_3 film on the sensor; (c) XPS spectra of the In 3d and O 1s region for In_2O_3 powder annealed at 320 °C.

sample at increasing concentrations. In the third setup, air was used as the background, and the breath sample was measured, and then increasing amounts of NH_3 was added in, all gases passing through a moisture trap at −20 to −25 °C.

3. Results

3.1. Characterization

The two semiconducting oxides of interest in this study are NiO and In_2O_3, were obtained from commercial sources. Detailed characterization is presented in Figs. 1 and 2 for NiO and In_2O_3 annealed at 320 °C, respectively.

3.1.1. NiO

The X-ray diffraction (XRD) pattern (Fig. 1a) is typical of the cubic structure of NiO (JCPDS No. 04-0835). Scanning electron microscopy (Fig. 1b) suggests particle diameters around 200–300 nm. X-ray photoelectron spectroscopy (XPS) of the O 1s region (Fig. 1c) suggests the presence of lattice oxygen

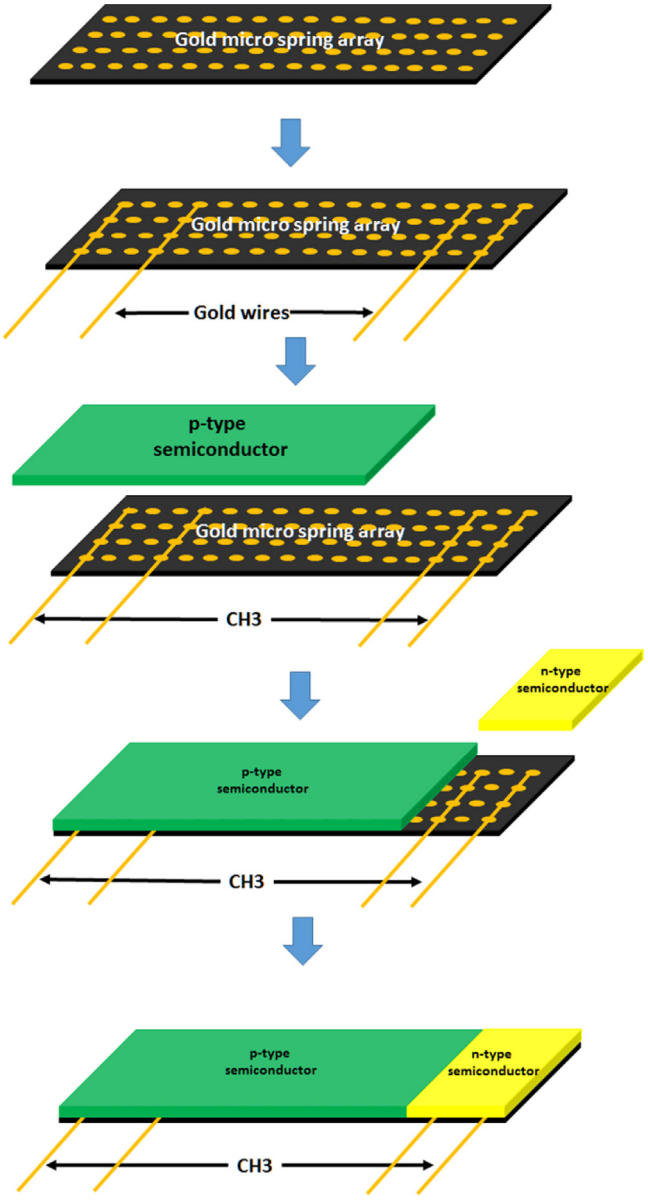

Fig. 3. Schematic representation of the steps of sensor fabrication.

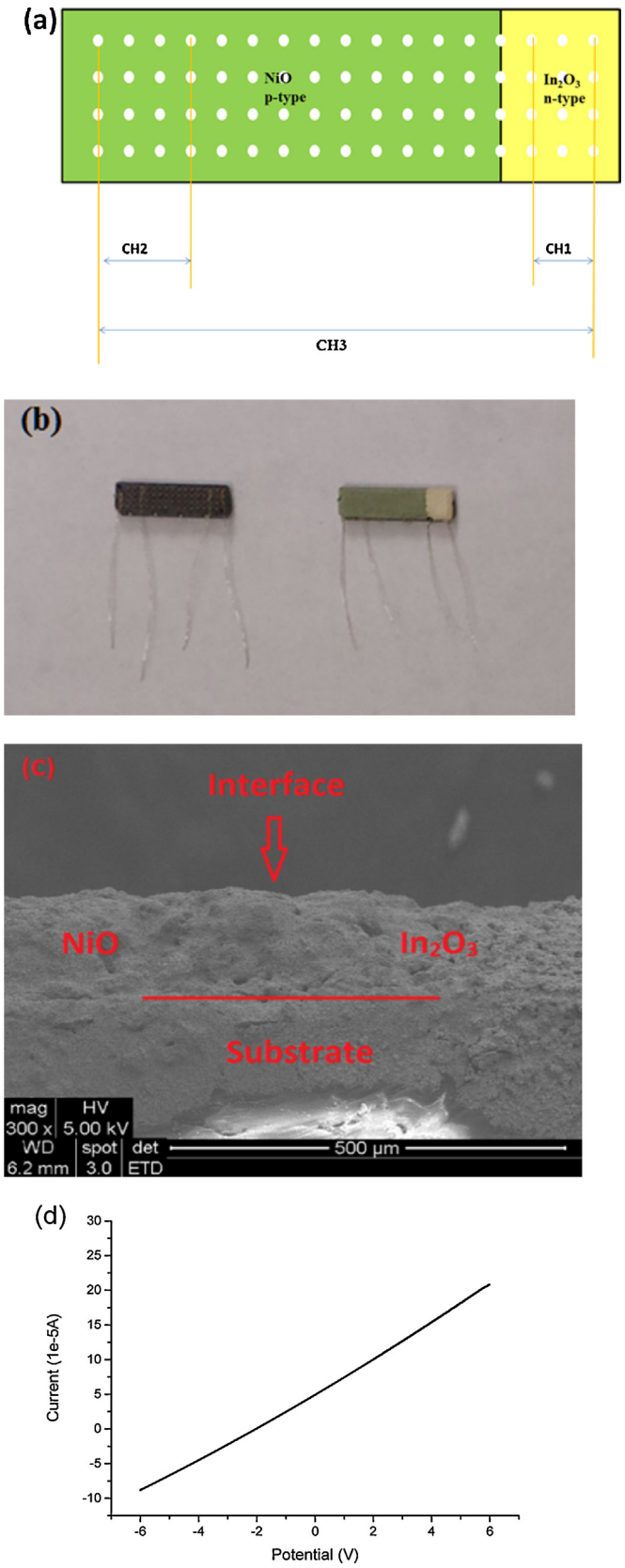

Fig. 4. (a) Schematic diagram of the sensor; (b) Photograph of bare sensor substrate with four gold wires (left) and sensor with adjacent NiO and In_2O_3 (right); (c) Side view SEM image of the sensor; (d) *I–V* characteristics across interface of NiO and In_2O_3 in 20% O_2/N_2 at 300 °C, scan rate = 0.1 V/s.

(O^{2-}, binding energy 529.4 eV), hydroxyl groups (binding energy 531 eV), and strongly chemisorbed oxygen (533 eV) [44,45]. In the nickel $2p_{3/2}$ region, peak at 853.7 is assigned to NiO_6 bulk cluster and peak at 855.8 eV to oxygen screened surface NiO_5 and nonlocal second neighbor screening of NiO_6 and NiO_5 [46,47]. The satellite region was fit to two peaks at 861.0 eV and 864.5 eV.

3.1.2. In_2O_3

XRD pattern of In_2O_3 shown in Fig. 2a is indicative of cubic crystalline structure (JCPDS No. 06-0416). Size of the particles from the SEM micrograph (Fig. 2b) is <100 nm. XPS (Fig. 2c) indicates two peaks at 444.7 and 452.2 eV assigned to In $3d_{5/2}$ and $3d_{3/2}$ states, typical of In^{3+} [48]. The O 1s spectra is asymmetric with two peaks at 530.2 and 532.0 eV, with the former assigned to the oxygen lattice state, and the broad envelop at 532.0 eV to oxygen ions in oxygen deficient-regions (vacancies) [48].

3.2. Sensor characteristics

3.2.1. Design

Fig. 3 shows a schematic of the steps involved in the sensor design, and Fig. 4 shows characteristics of the sensor. The two oxides are placed adjacent to each other on a plastic substrate and share a common interface. Substrate design makes it possible to measure resistances across varying lengths of the metal oxides (CH1 is defined as In_2O_3, CH2 as NiO and CH3 as a combination of both oxides, the choice of this combination is readily varied on the same sample). Fig. 4b shows a photograph of the sensor, with and without the oxide coating. The gold wires are used for the resistance measurements. Fig. 4c shows a side view of the sensor, indicating that the oxide films are ~200 μm thick. These devices are heated at 320 °C in air for 2 h, prior to making measurements at 300 °C. Fig. 4d is the current–voltage (I–V) plot at 300 °C and displays a linear relationship, indicating there is no rectification, as expected for a diffuse mixing of the powders [49].

3.2.2. Microstructure

Fig. 5a shows the top-view SEM of the NiO/In_2O_3 interface. The NiO side of the sensor is characterized by Raman bands at 500, 740, 900 and 1090 cm^{-1} (Fig. 5b), with the strongest bands at 500 and 1090 cm^{-1}, assigned to first and second order longitudinal optical modes, respectively [50]. On the In_2O_3 side, bands observed at 307, 366, 494 and 627 cm^{-1} (Fig. 5c) is consistent with previous literature [51]. Raman spectra were recorded along a 180 μm length across the interface and the intensities of Raman bands of NiO (500 cm^{-1}) and In_2O_3 (307 cm^{-1}) are plotted in Fig. 5d. There is intermixing of the two oxides over a ~30 μm distance at the interface.

3.3. Electrical characteristics

Fig. 6a is the resistance change of NiO after exposure to 1 ppm NH_3 at 300 °C. With the gas pulse on, there is a decrease in resistance, followed by a slow increase. After the gas pulse is turned off after 10 min, the resistance continues to increase for 10 min (crosses the baseline), followed by a slow decrease to the baseline over the next 25 min. Fig. 6b shows that if the NH_3 gas pulse is only on for 2 min at 300 °C, only a resistance decrease is observed, with both the response and recovery to the baseline occurring relatively rapidly (minutes). We use the 2 min exposure for all sensing experiments described later. At a temperature of 500 °C, the 1 ppm NH_3

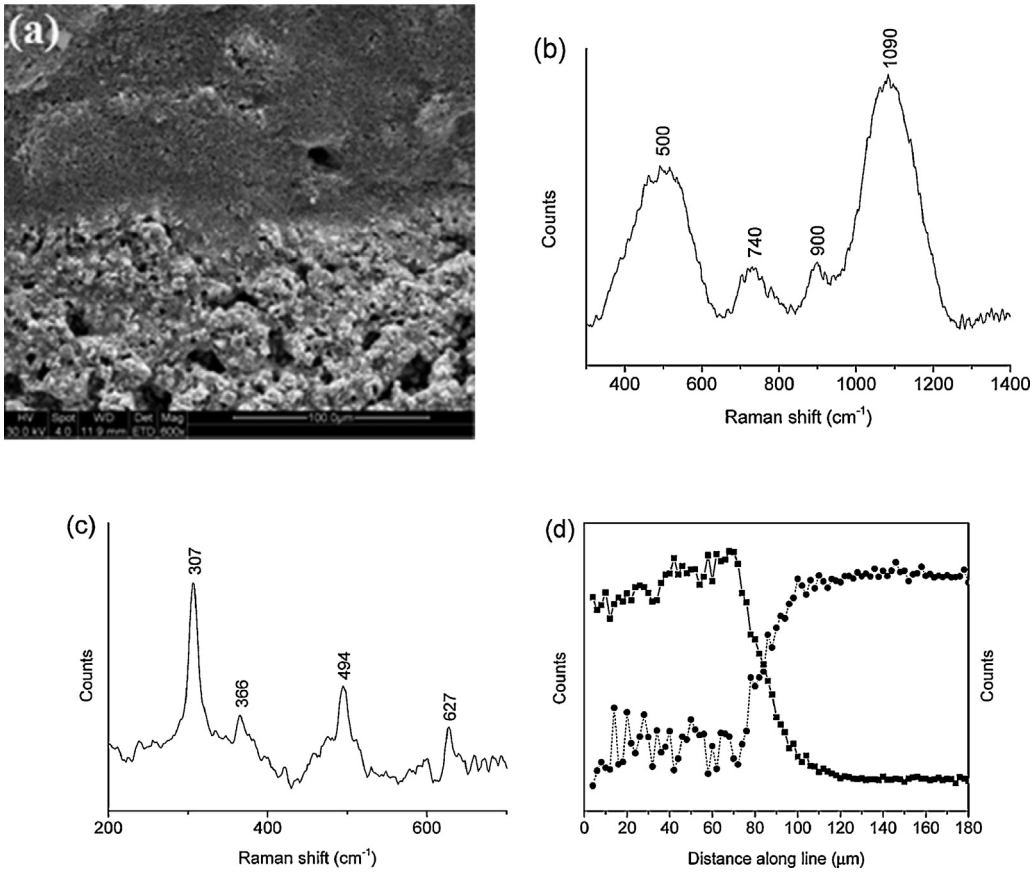

Fig. 5. (a) SEM image of interface between NiO (top) and In_2O_3 (bottom); (b) Raman spectra of NiO side; (c) Raman spectra of In_2O_3 side; (d) Integrated Raman intensities by mapping from In_2O_3 side to NiO side. In_2O_3: straight line with square markers; NiO: dashed line with circle markers.

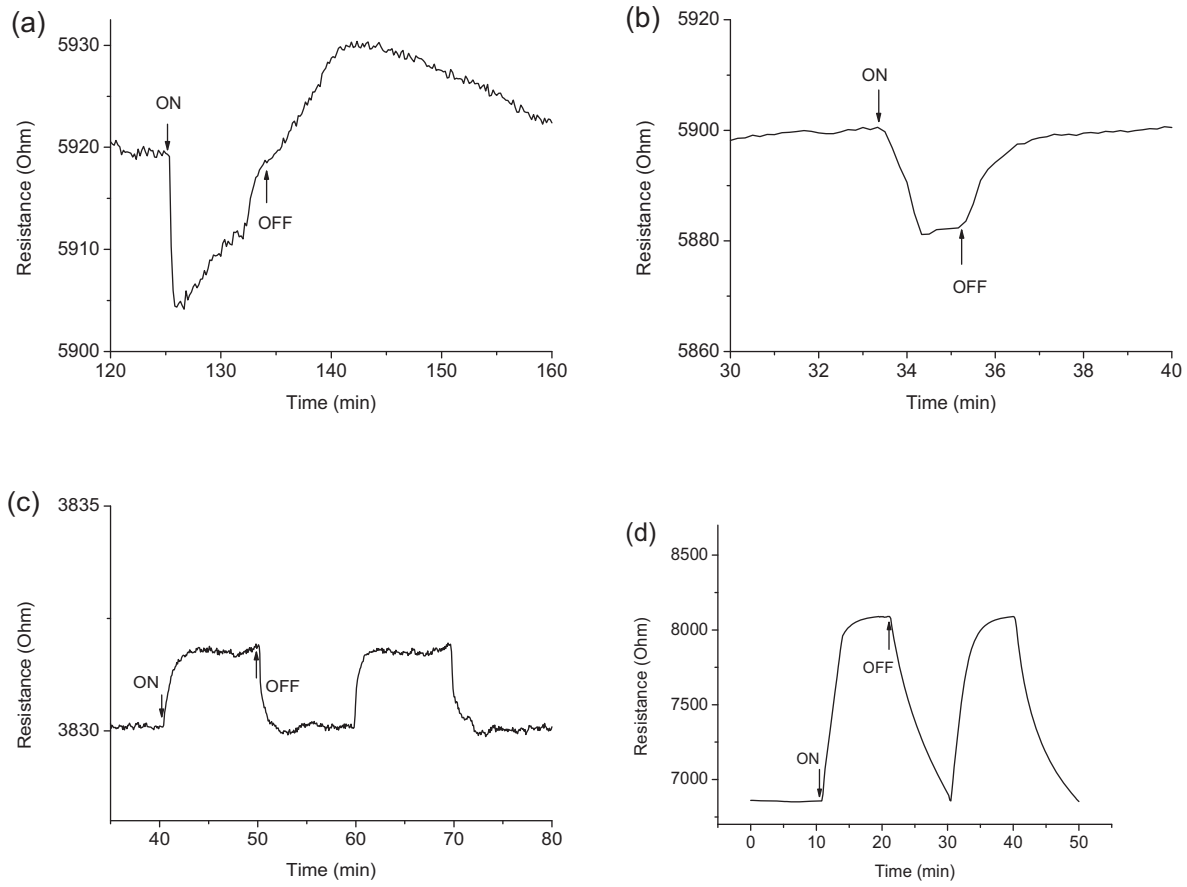

Fig. 6. Gas sensing characteristics of NiO for: (a) 1 ppm NH_3 at 300 °C with 10 min exposure time; (b) 1 ppm NH_3 at 300 °C with 2 min exposure time; (c) 1 ppm NH_3 at 500 °C with 10 min exposure time; (d) 10 ppm NH_3 at 300 °C with 10 min exposure time (20% O_2/N_2 as background).

registers a resistance increase (Fig. 6c). Fig. 6d shows an increase in resistance for 10 ppm NH_3 at 300 °C.

3.4. Infrared Spectroscopy

Infrared spectroscopy of the NiO surface was examined upon NH_3 exposure at 300 °C. Fig. 7a focuses on the 1220–1320 cm^{-1} spectral region, where we did observe changes with 1–10 ppm NH_3. With higher concentration of NH_3 (100 ppm), we did observe a band at 3220 cm^{-1} in the presence of oxygen (shown in Fig. S4). With N_2 passing over the NiO sample, there is no band in the 1200–1300 cm^{-1} region (Fig. 7a), but with 20% oxygen in the background gas, a band at 1267 cm^{-1} appears. With 1 ppm NH_3, there is an initial increase in this band (10 min) followed by a gradual decrease (30 min), which is reversed upon the removal of NH_3 with 20% O_2. Fig. 7b shows spectral changes with 10 ppm NH_3, with the intensity of the 1267 cm^{-1} band decreasing with time. Fig. 7c is a plot of the integrated intensity of the 1267 cm^{-1} band versus time with 1 and 10 ppm NH_3. The increase in the intensity of the 1267 cm^{-1} band is obvious with 1 ppm NH_3, though with the 10 ppm, the intensity increase is not as clear, though the decrease in intensity of this band with time is more marked. We discuss later the similar trends in resistance changes (Fig. 6a) and the intensity of the 1267 cm^{-1} peak (Fig. 7a).

3.5. Sensing characteristics

3.5.1. Carbon monoxide

All sensing experiments were done with 2 min pulses of the analyte gas. Fig. 8 shows the behavior of the integrated NiO–In_2O_3 sensor (Fig. 4a and b) towards pulses of CO (10, 3, 1 ppm). Resistance across three channels are shown, comprising In_2O_3 (CH1), NiO (CH2) and the In_2O_3–NiO combination (CH3). With CO, the In_2O_3 shows a decrease in resistance (n-type behavior), and with NiO, an increase in resistance (p-type behavior). With the appropriate inclusion of both oxides, the change in resistance in the presence of CO is severely reduced.

3.5.2. Nitric oxide

Fig. 9 shows the data with 5 and 10 ppb NO. Similar to the CO response, the NiO and the In_2O_3 show opposite responses (Fig. 9a and b), but because NO is an electron acceptor, the direction of the resistance change is reversed, as compared to CO. Nevertheless, when the two metal oxides are combined (CH3), the response to NO is minimized (Fig. 9c).

3.5.3. Ammonia

With NH_3 (1 ppm, 0.5 ppm, 0.1 ppm) on for a 2 min pulse, as shown in Fig. 10, both In_2O_3 and NiO show a decrease in resistance, and when both oxides are included, the signal even at 100 ppb remains significant.

3.5.4. Mixture of gases

These experiments were then repeated with both NH_3 and CO in the gas stream with the 2 min pulses of gas. Fig. 11 shows the results. With In_2O_3 (CH1), NH_3 (0.1, 0.5, 1 ppm) gives rise to a decrease in resistance. If CO (1, 3, 10 ppm) is included with the NH_3, the NH_3 signal is overwhelmed. Similar situation exists for NiO (CH2), except that a resistance increase is observed if CO is included in the gas pulse. However, the signal from the combination NiO–In_2O_3 channel (CH3) only exhibits a signal for NH_3, and the effect of CO, even at a concentration 100-fold higher than NH_3 is nullified.

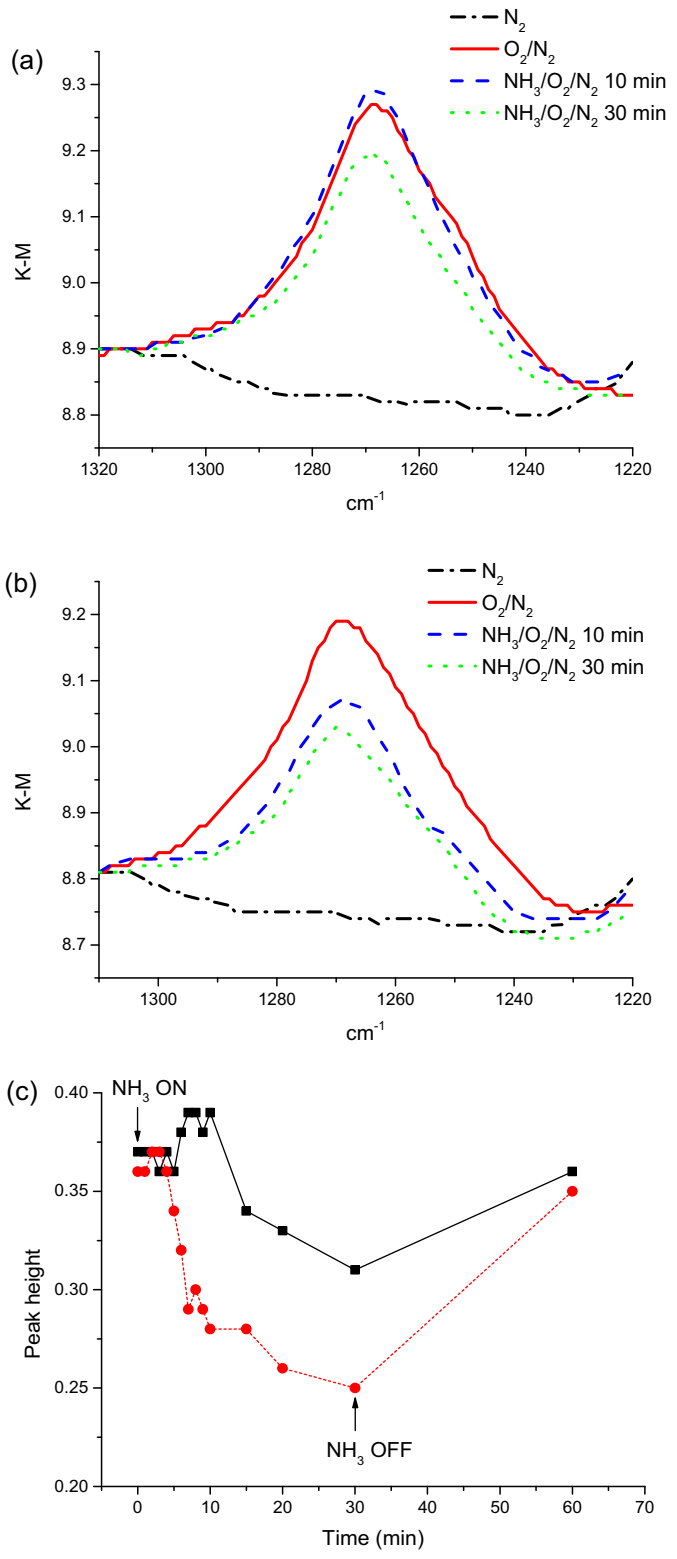

Fig. 7. In-situ infrared spectra of NiO at 300 °C in (a) 1 ppm NH_3; (b) 10 ppm NH_3; (c) time variation of relative peak height of the 1267 cm^{-1} band for 1 ppm (straight line) and 10 ppm (dashed line) NH_3.

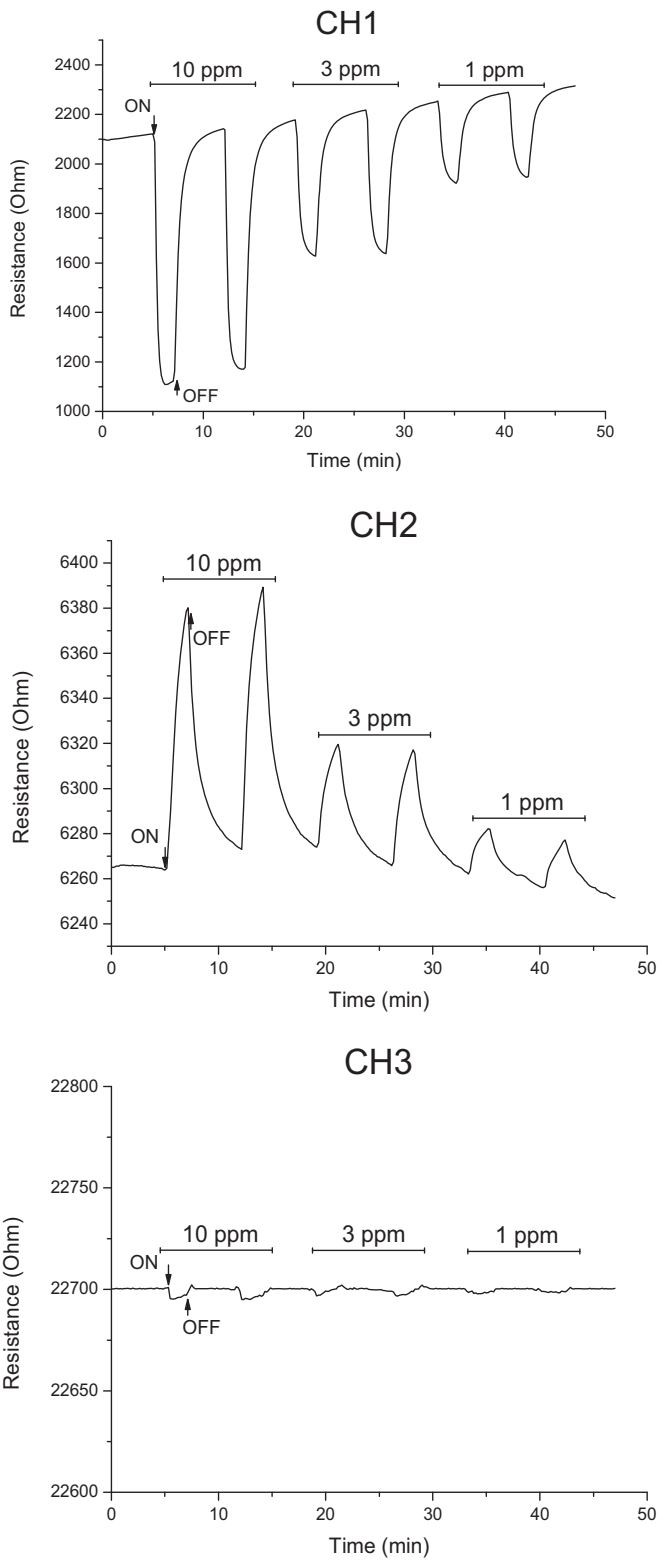

Fig. 8. Gas sensing characteristics of different sensing channels, In_2O_3 (CH1), NiO (CH2) and In_2O_3–NiO (CH3) for varying concentrations of CO at 300 °C (20% O_2/N_2 as background).

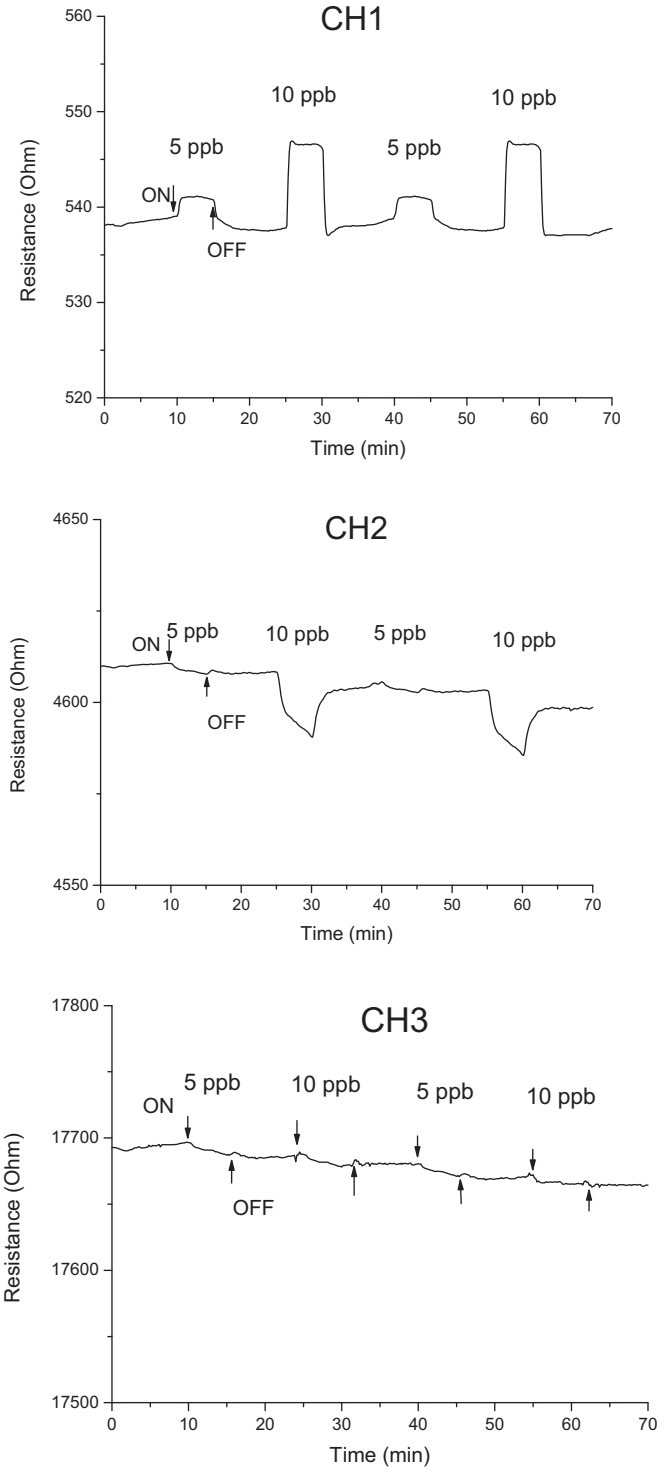

Fig. 9. Gas sensing characteristics of different sensing channels, In_2O_3 (CH1), NiO (CH2) and In_2O_3–NiO (CH3) for varying concentrations of NO at 300 °C (20% O_2/N_2 as background).

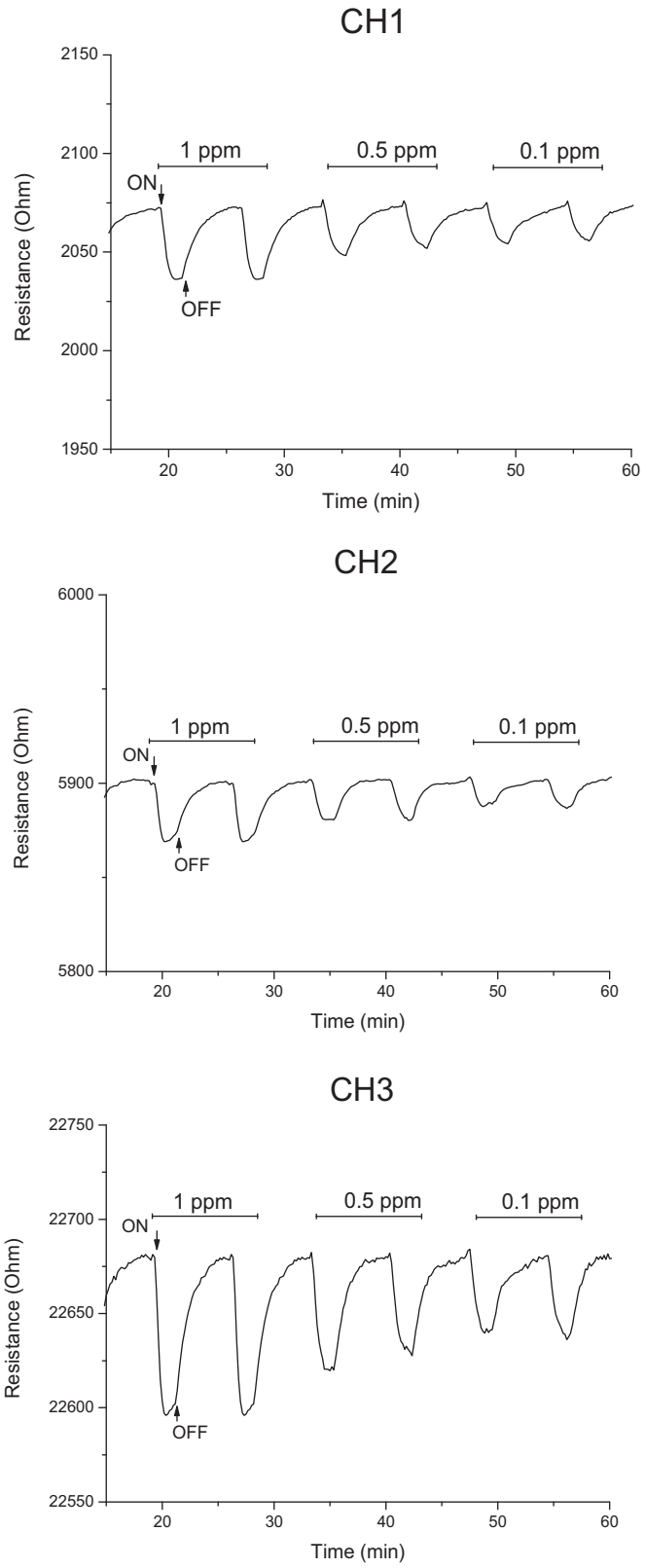

Fig. 10. Gas sensing characteristics of different sensing channels, In_2O_3 (CH1), NiO (CH2) and In_2O_3–NiO (CH3) for varying concentrations of NH_3 at 300 °C (20% O_2/N_2 as background).

3.6. Human breath samples

Three sets of experiments were carried out with human breath samples, and are schematically represented in Fig. 12.

3.6.1. Using breath as background

Breath samples were collected in Mylar bags, as previously described [52]. These samples were independently mixed via mass

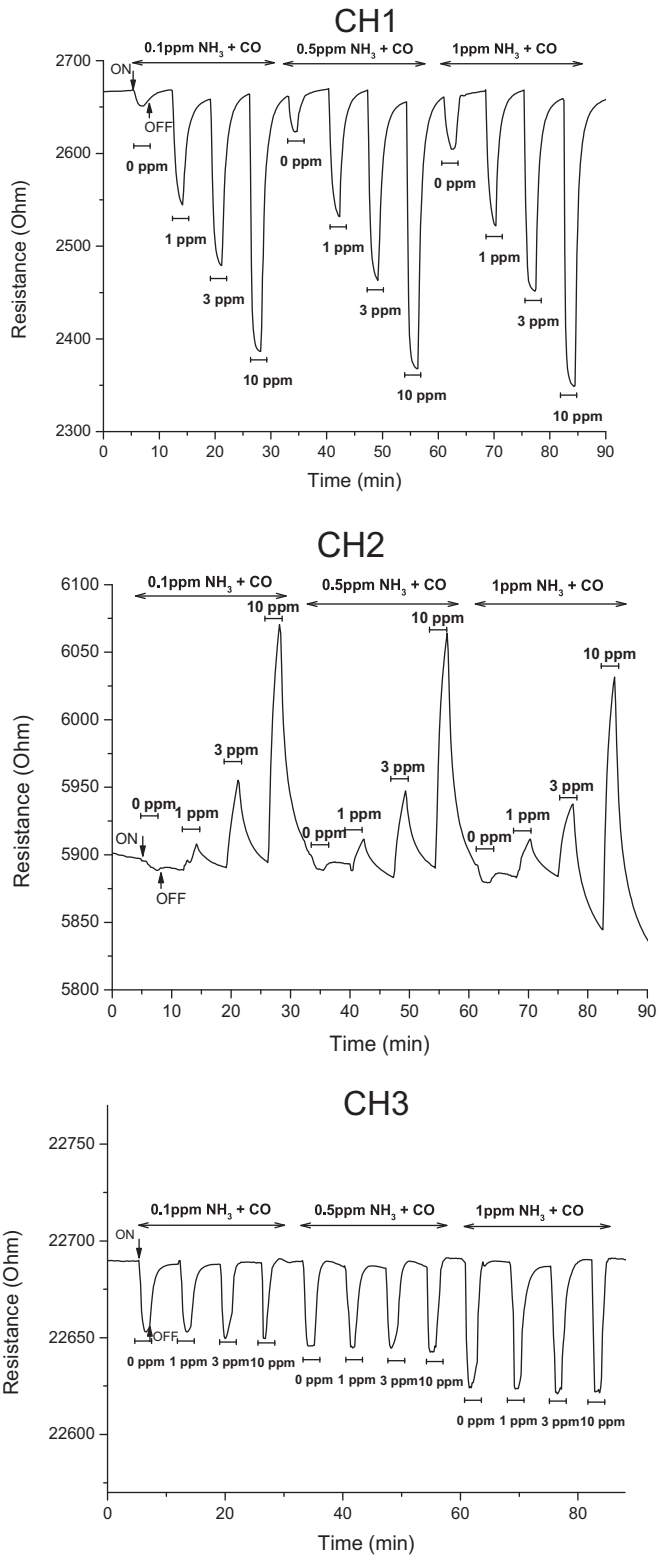

Fig. 11. Gas sensing characteristics of different sensing channels, In_2O_3 (CH1), NiO (CH2) and In_2O_3–NiO (CH3) for varying concentrations of NH_3/CO mixture at 300 °C (20% O_2/N_2 as background).

flow controllers with 10, 50, 100, 500, 1000 ppb of NH_3 and these samples were analyzed using the combined NiO–In_2O_3 sensor (CH3). In these experiments, the background signal was that of the breath alone, followed by introducing NH_3 in the gas mixture. The first experiment involved equilibrating the breath with water vapor at 37 °C with a measured relative humidity of 93% [15] (Fig. 12a), followed by the sensing measurement. The second experiment involved passing the breath through an ice bath resulting in a humidity of 30% (using apparatus in Fig. 12b). The third experiment involved passing the breath through a moisture trap at −20 to 25 °C, with a resulting humidity of 0% (Fig. 12b) The resulting sensing data using CH3 is shown in Fig. 13 (Figs. S1–S3 shows the data for all channels). With both the humid samples (Fig. 13a and b), the signal to NH_3 was poor. The presence of water influenced the sensing signal of NH_3 on both NiO and In_2O_3, particularly the former (Fig. S1), with the NiO exhibiting a resistance increase with NH_3, the opposite of the observation with dry gas (Fig. 10). With the breath sample mixed with NH_3 (bpt – 33.7 °C) passing through the −20 °C trap, the expected signal to the spiked NH_3 was realized (Fig. 13c). The calibration curve with the breath sample is shown in Fig. 13d, and indicates saturation with increasing concentrations.

3.6.2. *Using air as background*

In another set of experiments, air was used as the background (Fig. 12c), and a breath sample was measured using CH3 (all samples passing through the dry ice trap at −20 to −25 °C). Fig. 14a shows that the breath alone provides a signal, though we cannot ascertain what species are causing this signal. However, there was an increase in signal if the breath is mixed with NH_3, as shown in Fig. 14a. Such a standard addition experiment clearly indicates that the sensor is detecting NH_3. The background breath signal was normalized to R_o/R of 1, and the increased signal (measured as R_o/R) due to the spiked NH_3 is shown in Fig. 14b.

4. Discussion

In order to demonstrate the practical application of the sensor described in this paper, we chose to work with human breath sample. Detection of NH_3 in human breath at ~ppb levels can be helpful for diagnosis of various diseases. Typical concentrations for CO and NO in human breath are at ppm and ppb levels, respectively [43]. The outcome of this study is a sensor that can detect NH_3 at low concentrations (<1000 ppb) with selectivity against CO at ppm and NO at ppb levels.

The sensor design used in this study is similar to our recent report on NO sensors [43]. The concept is to use a mixture of p- and n-type semiconducting oxide, but physically separated with a common interface (Figs. 3 and 4). The separated p and n-oxides allows for altering the contribution of each oxide to the resistance more readily than physical mixture of powders.

The two oxides examined here are n-type In_2O_3 and p-type NiO. The conduction model for both n-type and p-type metal oxide gas sensors have been reviewed [53–55]. In both n- and p-type oxides, oxygen ionosorption plays a key role in the sensing paradigm. In the case of n-type, such chemisorption leads to a decrease of majority carrier electrons at the surface of grains, whereas in p-type oxides, the oxygen ionosorption leads to a surface accumulation of holes. In n-type oxides, conduction is through the bulk of the oxide, whereas in p-type, conduction is along the surface. Under certain conditions, resistance changes from n- to p-type and vice versa has been observed. This effect is observed on Fe_2O_3, MoO_3, In_2O_3, SnO_2, TeO_2 and TiO_2, and several explanations have been proposed, including formation of a surface inversion layer driven via surface adsorption, different types of surface reactions, influence of polymorphs and morphology, as well as the effect of ionic dopants/impurities [29,56–61].

The resistance changes of NiO and In_2O_3 to CO and NO were as expected (Figs. 8a and b and 9a and b). NiO is behaving as a

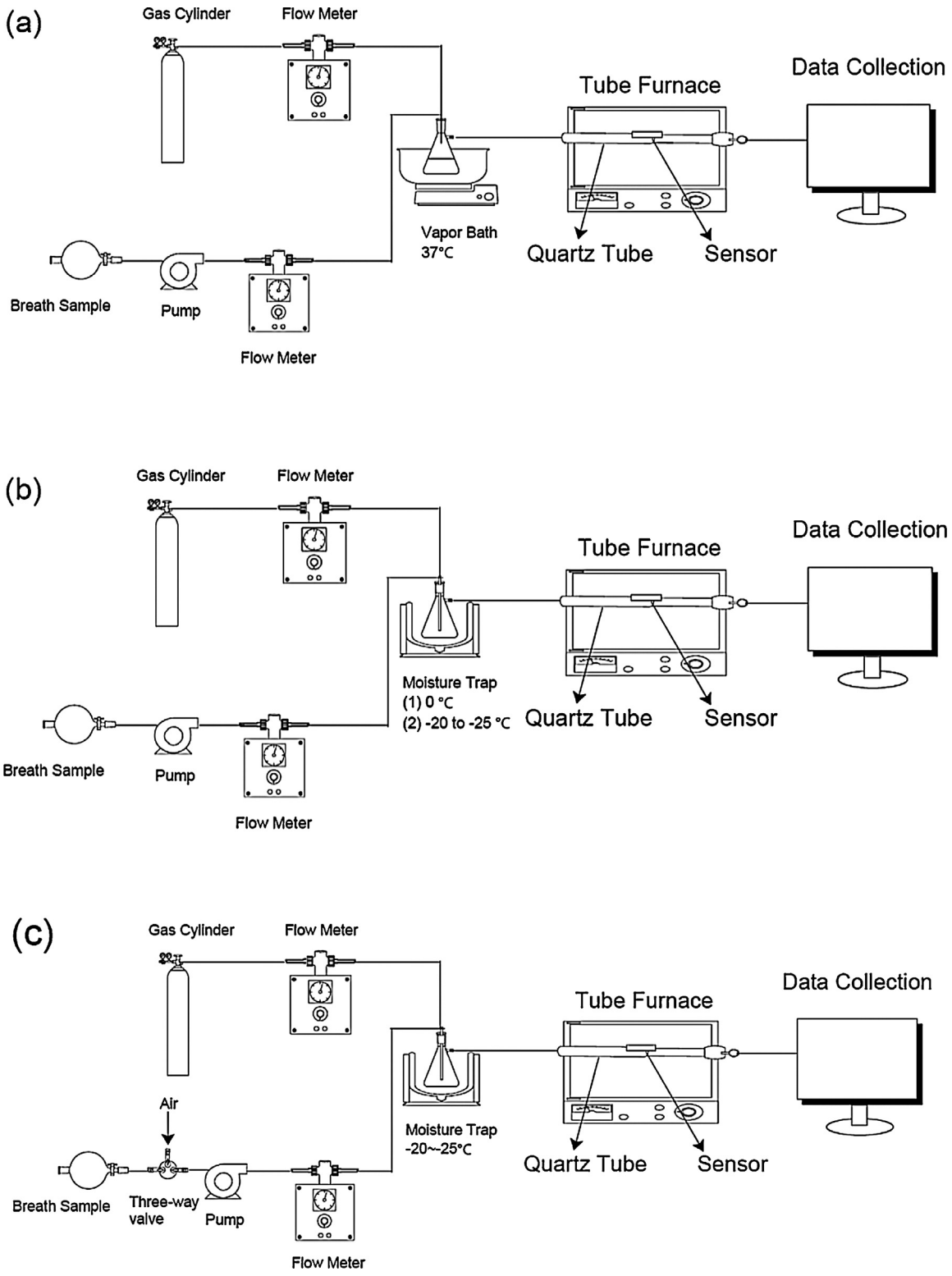

Fig. 12. Schematic diagram of the simulated breath system (a) with 37 °C vapor bath; (b) with moisture trap; (using breath as background) (c) using air as background, and with moisture trap.

p-type semiconductor, with hole conduction as the main contribution. CO reacts with chemisorbed oxygen on the oxide surface releasing electrons, which raise the resistance of p-type NiO and lowers the resistance of n-type In_2O_3. With the appropriate contributions from both oxides, the resistance change to CO can be nullified (Fig. 8c). Similar observations are made with NO (Fig. 9c).

Under conditions in which NH_3 can react with chemisorbed oxygen, it usually behaves as a reducing gas, with proposed reactions such as [62]

$$2NH_3 + 3O^- \rightarrow N_2 + 3H_2O + 3e \quad (1)$$

$$2NH_3 + 5O^- \rightarrow 2NO + 3H_2O + 5e \quad (2)$$

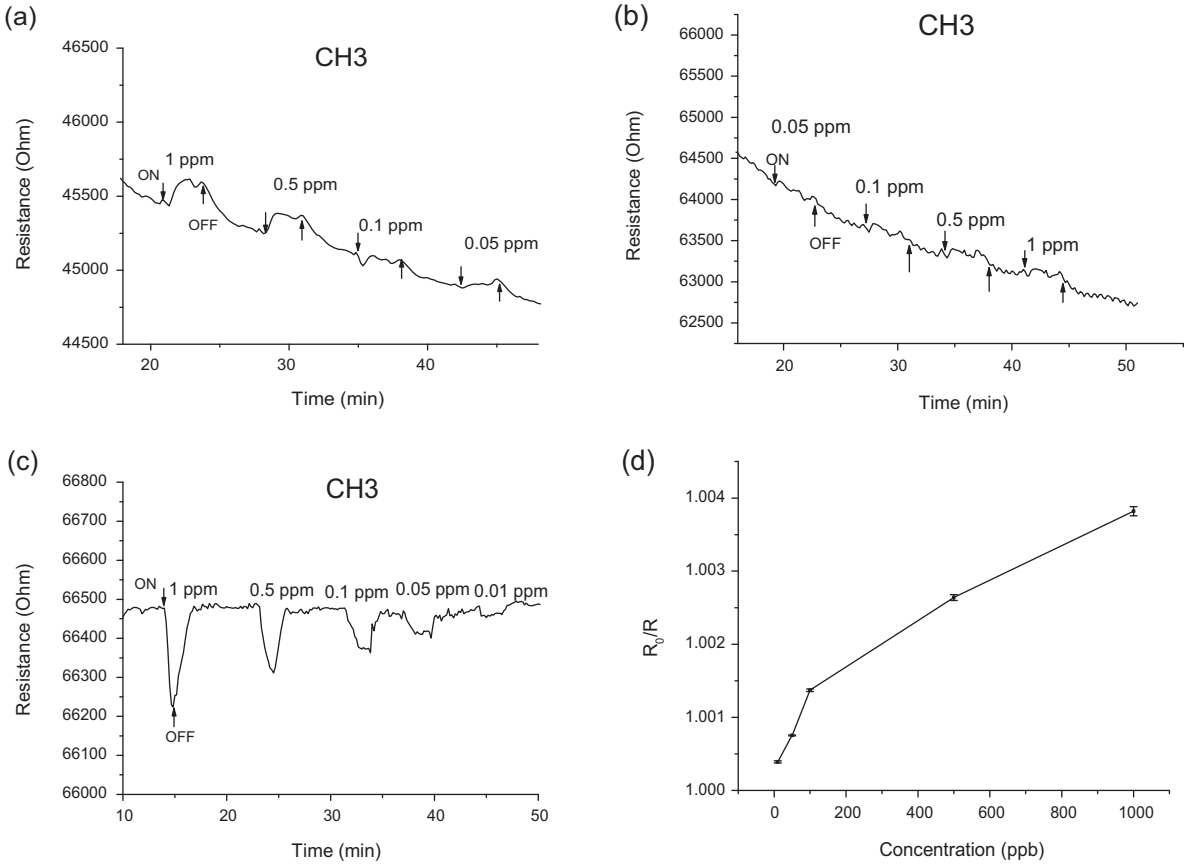

Fig. 13. Gas sensing characteristics of sensing channel CH3 (In_2O_3–NiO) for breath sample containing added concentrations of NH_3 at 300 °C (a) with 37 °C vapor bath; (b) with ice bath (c) with dry ice/acetonitrile moisture trap; (d) Calibration curve for relative resistance changes (R_0/R) of CH3 for varying concentrations of NH_3 added to breath sample (breath sample without spiked NH_3 used as background).

These reactions are more favorable at higher temperature. The resistance changes upon interaction of NH_3 with metal oxides can be anomalous. For n-type oxides, such as In_2O_3 and WO_3, at lower temperatures (<300 °C), there is a resistance decrease. However at higher temperatures, initial resistance decrease is followed by a resistance increase [62–65]. For n-type semiconductors, NO, the product of NH_3 oxidation upon chemisorption will lead to an increase in resistance. This competition between NH_3 oxidation and NO chemisorption is used to explain the anomalous sensing behavior. For avoiding the anomalous sensing behavior due to NO_x, low temperature operation or the use of catalysts have been suggested [66]. Other explanations for anomalous behavior, as in hexagonal-WO_3 have been ascribed to the formation of an inversion layer [67].

Our data on In_2O_3 at 300 °C indicates that NH_3 is behaving as a reducing gas (Fig. 10a), with a decrease in resistance, as has been observed by others [24,68]. The resistance changes with NH_3 on p-type NiO is more complicated. The resistance increase observed 500 °C with 1 ppm NH_3 (Fig. 6c) and 10 ppm NH_3 at 300 °C (Fig. 6d) is explained by reactions (1) and (2), where the electrons created upon NH_3 oxidation combine with the majority carrier holes, and lead to an increase in resistance, consistent with previous studies on NiO with 20–50 ppm NH_3 [31]. The behavior with 1 ppm NH_3 at 300 °C is not as expected and needs a different interpretation. As shown in Fig. 6a, there is an initial decrease in resistance over the first few minutes, followed by a gradual increase. Differences in direction of resistance changes as a function of analyte concentrations has been noted. On p-type TeO_2 at low temperatures (80 °C), a resistance decrease with ethanol (<300 ppm), an anomalous behavior, whereas with higher concentrations of ethanol, the resistance increased, as expected for a reducing gas on a p-type material has been reported [59]. For p-type CuO nanowires, with NO_2 an oxidizing gas, at concentration <5 ppm, the resistance increased (anomalous behavior), whereas with 30–100 ppm NO_2, the resistance decreased, as expected for an oxidizing gas and p-type material [69]. No clear mechanistic information for such behavior is available in the literature.

The in-situ IR spectra shown in Fig. 7 provide some clues. Formation of a band at 1267 cm^{-1} on NiO is observed as gas is switched from N_2 to 20% O_2 at 300 °C (Fig. 7a and c). This band disappears if the O_2 is replaced with N_2, so we assign this band to chemisorbed oxygen species. Upon introduction of 1 ppm NH_3, there is an increase in intensity of this band, followed by a decrease. The change in intensity of the 1267 cm^{-1} band in Fig. 7c in the presence of 1 ppm NH_3 mirrors the change in conductivity upon 1 ppm NH_3 exposure to NiO, as shown in Fig. 6a (the timings do not exactly overlap since the IR was done on a powdered sample).

Several previous studies have noted a band in the 1200–1300 cm^{-1} region upon oxygen chemisorption on metal oxides [70]. On Fe_2O_3, bands between 1250 and 1350 cm^{-1} have been assigned to perturbed O_2^- species, and in particular, the band at 1270 cm^{-1} is prominent and stable up to 300 °C [71]. There are few infrared studies of oxygen adsorption on NiO, bands at 1070 and 1140 cm^{-1} were observed at 77 K and assigned to O_2^- [70]. On Fe_2O_3, bands in the 900–1100 cm^{-1} were assigned to O_2^{2-} species [72]. Formation of O^- on NiO has been proposed, though no distinct infrared bands were identified [72]. Peroxo species (O_2^{2-}) have been proposed upon oxygen adsorption on NiO [73]. On CuCl and CuBr, a band around 1270 cm^{-1} has been assigned to O_2 coordinated with Cu^+, and intensity of this infrared band also

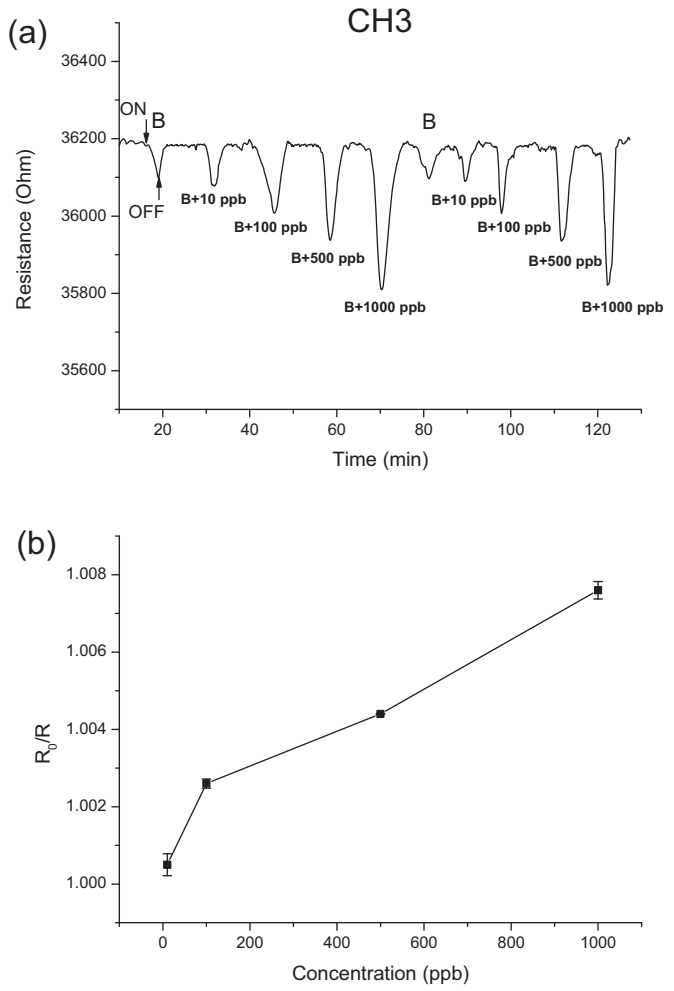

Fig. 14. (a) Gas sensing characteristics of sensing channel CH3 (In_2O_3–NiO) for breath sample B and then with added NH_3 (10–1000 ppb) at 300 °C with dry ice/acetonitrile moisture trap; (b) Calibration curve for relative resistance changes (R_0/R) of CH3 for varying concentrations of NH_3 in breath sample (air as background).

decreased upon exposure to NH_3 [74]. Based on these studies, we assign the band at 1267 cm^{-1} (Fig. 7a and b) on NiO to O_2^-.

The reactivity of NH_3 on metal oxide surfaces is enhanced in the presence of oxygen. On Mg (0 0 0 1) surface, NH_3 was reactive with the surface only in the presence of oxygen [75]. Chemisorbed oxygen on Ni (1 1 0) and Ni (1 0 0) is reactive with NH_3 with H abstraction and formation of NH_x species [76]. Surface spectroscopic studies have shown the high reactivity of NH_3 with adsorbed oxygen on Ni (1 1 1) [77].

It has been proposed that the O_2^- is in equilibrium with O^- [75]

$$O_2^- \rightleftarrows O^- + O \quad (3)$$

NH_3 chemisorption at lower temperatures is proposed to lead to NH_2 and OH^- via reaction with the O^- [75]

$$M^{x+}\cdots NH_3 + O^- \rightarrow M^{x+}\cdots NH_2 + OH^- \quad (4)$$

Ammonia adsorption on alumina surface (acid/base sites) was proposed to lead to NH_2 and OH formation for about 10% of all the NH_3 molecules that are absorbed [78]. Bands due to NH_2 were reported at 3386 and 3355 cm^{-1} [76]. Dissociative chemisorption of NH_3 to NH_2 and OH driven by oxygen functionality is noted on epoxide groups in reduced graphene oxide, with vibrational bands assigned as 3208, 3270 cm^{-1} (NH_2) and 3400 cm^{-1} (OH) [79]. With the 1 ppm NH_3 on NiO, we did not observe any bands due to NH_2, but with 100 ppm NH_3 on NiO at 300 °C, and subsequent cooling to room temperature, a band appears at 3220 cm^{-1} in the presence of O_2, but not in the presence of only N_2 (these spectra are shown in Fig. S4). We assign the 3220 cm^{-1} band to N–H stretching.

Based on these observations, we explain the anomalous behavior of 1 ppm NH_3 observed in Fig. 6a. We hypothesize that reactions (3) and (4) will take place on the NiO surface (we have IR evidence for the O_2^- species), and with (4) occurring, it will lead to more O_2 chemisorption as O_2^-, as O^- is used up in reaction (4). IR indicates transient increase of the O_2^- band upon exposure to NH_3 (Fig. 7a). With increased O_2 chemisorption as O_2^-, it will lead to a decrease in resistance. The increase in resistance observed later occurs due to subsequent reactions (1) and (2) due to oxidation of NH_3. At higher temperatures, or with higher concentrations of NH_3, the transient decrease in resistance is not observed (Fig. 6c and d) as reactions (1) and (2) are promoted.

We have exploited the transient decrease in resistance upon exposure of low levels of NH_3 on NiO for amplifying the sensor signal. This was done by exposing the NiO to only 2 min of NH_3 thus giving time for the chemisorption effects to occur (reactions (3) and (4), Fig. 6b), but not the chemical reactions (reactions (1) and (2)). The resistance of NiO decreases and then recovers quite rapidly, as compared to the 10 min exposure, where the products of the chemical reaction form and need to be desorbed, before the sensor baseline is reached, and at 300 °C, takes 40 min. With the 2 min NH_3 exposure, both NiO and In_2O_3 show a decrease in resistance, so the sensing data that combines both oxides (CH3) lead to an additive effect, amplifying the response from NH_3 (Fig. 10) while with CO and NO, the opposite response lead to a cancellation of signal (Figs. 8 and 9). This strategy allows us to sense the presence of NH_3 in the concentration range of NH_3 in the concentration range <1000 ppb, in the presence of CO as seen in Fig. 11.

Since the need for detecting NH_3 in human breath is of the order of hundreds of ppb, we used breath samples as a possible application of this sensor. The high humidity in breath posed a significant interference (Fig. 13a and b), and only upon removal of water from the breath by a cold trap (−20 °C), the signal due to NH_3 could be retrieved (Fig. 13c). Since NH_3 and H_2O can both act as Lewis bases, it is not surprising that humidity poses an interference to NH_3. Interference to humidity not only is present for NH_3 [80], but to other gases such as CO [81], and for both n- and p-type materials. Chemisorption of water can follow the same as reaction (4), leading to formation of hydroxyl groups [53], with M^{x+}–OH bond formation. The observation that in the presence of water, there is an increase in resistance of NiO to NH_3 (Fig. S1) indicates that the water adsorption disrupts the oxygen chemisorption as O_2^-, possibly by adsorbing at these sites. Thus, the p–n oxide arrangement can minimize interferences from other gases, such as CO, but because of the pronounced water interaction with the oxides, in general, humidity will be a strong interference to NH_3.

By removing the humidity, the sensor can detect NH_3 that is mixed into the breath. We have done the breath + NH_3 experiments in two ways. The breath is used as the background sample, and any increase in NH_3 in breath can be measured (Fig. 13cd). Or, the breath can be measured using air as the background sample, the breath alone gives a signal and then any increase in NH_3 can be measured from the increased signal (Fig. 14a and b). The possible biomedical application we see of this sensor is measuring an increase of NH_3 in breath. For *H. Pylori* infection diagnosis, the current standard of measurement involves feeding the patient a sample of 13C or 14C-labeled urea. The urease in the stomach (due to the bacteria) decomposes the urea to $^{13}CO_2$ or $^{14}CO_2$ and NH_3. The radioactive $^{14}CO_2$ in breath is then measured [82]. With $^{13}CO_2$, a mass spectrometer is necessary to carry out the measurement [82]. Because the sensor we have developed can measure NH_3 at ppb levels, the strategy would be to feed the patient regular urea and measure the released NH_3. There would still be the need of the humidity trap

to remove water. The trap can remove other organic volatiles in breath, but is not an issue in the application we are proposing for this sensor. Gases such as CO and NO (along with the NH_3) will still come through the trap, and the p-n strategy as outlined in this paper minimizes the influence of these interferents, while enhancing the signal for NH_3.

5. Conclusions

This study demonstrates the concept of using p-type of NiO and n-type In_2O_3 placed side-by-side on a substrate with common interface as a sensor platform. The adjacent placement of the oxides allows for ease of variation of the amount of oxide to be included for making the resistance measurements in the presence of analyte gas. With this strategy, the change in resistance with 3–10 ppm CO was almost nil, since In_2O_3 and NiO give opposite responses to CO. Ammonia is also a reducing gas, but at low concentrations of NH_3 (<1 ppm) at 300 °C, the response with In_2O_3 was as expected (resistance decrease), but with NiO, the resistance change was anomalous. For the first 8 min of a 10 min exposure to NH_3, there was a resistance decrease followed by a gradual resistance increase over the next 20 min, followed by a 10 min decrease to baseline resistance. With the help of in-situ infrared spectroscopy, this behavior was correlated with NH_3 chemisorption and involvement of O_2^- species. Advantage was taken of the transient decrease with NH_3 on NiO to design a sensor that shows a resistance decrease for both NiO and In_2O_3 by controlling the gas pulses to a duration of 2 min. With this strategy, combining the two oxides enhanced the signal of NH_3, allowing ready detection at 100 ppb concentration. These sensors were used to detect NH_3 that was mixed with human breath. As long as the humidity is completely removed from the breath sample, 10–1000 ppb of added ammonia could be detected. Water interference arises from competing reactions with O_2^- and the transient decrease in resistance with NH_3 on NiO is no longer observed, thus removing the amplification. A potential application of such a sensor would be in *H.Pylori* diagnosis.

Appendix A. Supplementary data

Supplementary data associated with this article can be found, in the online version, at http://dx.doi.org/10.1016/j.snb.2015.11.085.

References

[1] B. Timmer, W. Olthuis, A. van den Berg, Ammonia sensors and their applications – a review, Sensors and Actuators B: Chemical 107 (2005) 666–677.
[2] J. Pauluhn, Acute inhalation toxicity of ammonia: revisiting the importance of RD50 and LCT01/50 relationships for setting emergency response guideline values, Regulatory Toxicology and Pharmacology 66 (2013) 315–325.
[3] A.R. Tonelli, A. Pham, Bronchiectasis, a long-term sequela of ammonia inhalation: a case report and review of the literature, Burns 35 (2009) 451–453.
[4] S. DuBois, S. Eng, R. Bhattacharya, S. Rulyak, T. Hubbard, D. Putnam, D.J. Kearney, Breath ammonia testing for diagnosis of hepatic encephalopathy, Digestive Diseases and Sciences 50 (2005) 1780–1784.
[5] D.J. Kearney, T. Hubbard, D. Putnam, Breath ammonia measurement in Helicobacter pylori infection, Digestive Diseases and Sciences 47 (2002) 2523–2530.
[6] A. Amano, Y. Yoshida, T. Oho, T. Koga, Monitoring ammonia to assess halitosis, Oral Surgery Oral Medicine Oral Pathology Oral Radiology and Endodontics 94 (2002) 692–696.
[7] C. Di Natale, R. Paolesse, E. Martinelli, R. Capuano, Solid-state gas sensors for breath analysis: a review, Analytica Chimica Acta 824 (2014) 1–17.
[8] U. Lachish, S. Rotter, E. Adler, U. El-Hanany, Tunable diode laser based spectroscopic system for ammonia detection in human respiration, Review of Scientific Instruments 58 (1987) 923.
[9] J. Manne, O. Sukhorukov, W. Jager, J. Tulip, Pulsed quantum cascade laser-based cavity ring-down spectroscopy for ammonia detection in breath, Applied Optics 45 (2006) 9230–9237.
[10] H. Ishida, T. Satou, K. Tsuji, N. Kawashima, H. Takemura, Y. Kosaki, S. Shiratori, T. Agishi, The breath ammonia measurement of the hemodialysis with a QCM-NH_3 sensor, Bio-Medical Materials & Engineering 18 (2008) 99–106.
[11] K. Toda, J. Li, P.K. Dasgupta, Measurement of ammonia in human breath with a liquid-film conductivity sensor, Analytical Chemistry 78 (2006) 7284–7291.
[12] A.D. Aguilar, E.S. Forzani, L.A. Nagahara, I. Amlani, R. Tsui, N.J. Tao, Breath ammonia sensor based on conducting polymer nanojunctions, IEEE Sensors Journal 8 (2008) 269–273.
[13] T. Hibbard, K. Crowley, A.J. Killard, Direct measurement of ammonia in simulated human breath using an inkjet-printed polyaniline nanoparticle sensor, Analytica Chimica Acta 779 (2013) 56–63.
[14] M.-Z. Dai, Y.-L. Lin, H.-C. Lin, H.-W. Zan, K.-T. Chang, H.-F. Meng, J.-W. Liao, M.-J. Tsai, H. Cheng, Highly sensitive ammonia sensor with organic vertical nanojunctions for noninvasive detection of hepatic injury, Analytical Chemistry 85 (2013) 3110–3117.
[15] T. Hibbard, K. Crowley, F. Kelly, F. Ward, J. Holian, A. Watson, A.J. Killard, Point of care monitoring of hemodialysis patients with a breath ammonia measurement device based on printed polyaniline nanoparticle sensors, Analytical Chemistry 85 (2013) 12158–12165.
[16] J. Gong, Y. Li, Z. Hu, Z. Zhou, Y. Deng, Ultrasensitive NH_3 gas sensor from polyaniline nanograin enchased TiO_2 fibers, Journal of Physical Chemistry C 114 (2010) 9970–9974.
[17] S. Davies, P. Spanel, D. Smith, Quantitative analysis of ammonia on the breath of patients in end-stage renal failure, Kidney International 52 (1997) 223–228.
[18] M. Norman, C. Spirig, V. Wolff, I. Trebs, C. Flechard, A. Wisthaler, R. Schnitzhofer, A. Hansel, A. Neftel, Intercomparison of ammonia measurement techniques at an intensively managed grassland site (Oensingen, Switzerland), Atmospheric Chemistry and Physics 9 (2009) 2635–2645.
[19] G. Wang, Y. Ji, X. Huang, X. Yang, P.-I. Gouma, M. Dudley, Fabrication and characterization of polycrystalline WO_3 nanofibers and their application for ammonia sensing, Journal of Physical Chemistry B 110 (2006) 23777–23782.
[20] B.T. Marquis, J.F. Vetelino, A semiconducting metal oxide sensor array for the detection of NO_x and NH_3, Sensors and Actuators B: Chemical 77 (2001) 100–110.
[21] E. Llobet, G. Molas, P. Molinas, J. Calderer, X. Vilanova, J. Brezmes, J.E. Sueiras, X. Correig, Fabrication of highly selective tungsten oxide ammonia sensors, Journal of the Electrochemical Society 147 (2000) 776–779.
[22] J. Zhang, S. Wang, M. Xu, Y. Wang, H. Xia, S. Zhang, X. Guo, S. Wu, Polypyrrole-coated SnO_2 hollow spheres and their application for ammonia sensor, Journal of Physical Chemistry C 113 (2009) 1662–1665.
[23] N. Van Hieu, L.T.B. Thuy, N.D. Chien, Highly sensitive thin film NH_3 gas sensor operating at room temperature based on SnO_2/MWCNTs composite, Sensors and Actuators B: Chemical 129 (2008) 888–895.
[24] C. Li, D.H. Zhang, B. Lei, S. Han, X.L. Liu, C.W. Zhou, Surface treatment and doping dependence of In_2O_3 nanowires as ammonia sensors, Journal of Physical Chemistry B 107 (2003) 12451–12455.
[25] S. Elouali, L.G. Bloor, R. Binions, I.P. Parkin, C.J. Carmalt, J.A. Darr, Gas sensing with nano-indium oxides (In_2O_3) prepared via continuous hydrothermal flow synthesis, Langmuir 28 (2012) 1879–1885.
[26] J.B. Law, J.T. Thong, Improving the NH_3 gas sensitivity of ZnO nanowire sensors by reducing the carrier concentration, Nanotechnology 19 (2008) 205502.
[27] S.L. Patil, S.G. Pawar, A.T. Mane, M.A. Chougule, V.B. Patil, Nanocrystalline ZnO thin films: optoelectronic and gas sensing properties, Journal of Materials Science: Materials in Electronics 21 (2010) 1332–1336.
[28] S.G. Pawar, S.L. Patil, M.A. Chougule, B.T. Raut, S.A. Pawar, R.N. Mulik, V.B. Patil, Nanocrystalline TiO_2 thin films for NH_3 monitoring: microstructural and physical characterization, Journal of Materials Science: Materials in Electronics 23 (2011) 273–279.
[29] A.K. Prasad, D.J. Kubinski, P.I. Gouma, Comparison of sol-gel and ion beam deposited MoO_3 thin film gas sensors for selective ammonia detection, Sensors and Actuators B: Chemical 93 (2003) 25–30.
[30] P.T. Moseley, D.E. Williams, A selective ammonia sensor, Sensors and Actuators B: Chemical 1 (1990) 113–115.
[31] J. Wang, P. Yang, X. Wei, Z. Zhou, Preparation of NiO two-dimensional grainy films and their high-performance gas sensors for ammonia detection, Nanoscale Research Letters 10 (2015).
[32] I. Singh, R.K. Bedi, Influence of pH on the synthesis and characterization of CuO powder for thick film room-temperature NH_3 gas sensor, Journal of Materials Science 46 (2011) 5568–5580.
[33] V. Srivastava, K. Jain, Highly sensitive NH_3 sensor using Pt catalyzed silica coating over WO_3 thick films, Sensors and Actuators B: Chemical 133 (2008) 46–52.
[34] F. Winquist, Modified palladium metal-oxide-semiconductor structures with increased ammonia gas sensitivity, Applied Physics Letters 43 (1983) 839.
[35] T. Maekawa, J. Tamaki, N. Miura, N. Yamazoe, Gold-loaded tungsten-oxide sensor for detection of ammonia in air, Chemistry Letters (1992) 639–642.
[36] H. Guo, S. Tao, Silver nanoparticles doped silica nanocomposites coated on an optical fiber for ammonia sensing, Sensors and Actuators B: Chemical 123 (2007) 578–582.
[37] P. Gouma, K. Kalyanasundaram, X. Yun, M. Stanacevic, L.S. Wang, Nanosensor and breath analyzer for ammonia detection in exhaled human breath, IEEE Sensors Journal 10 (2010) 49–53.
[38] N. Savage, B. Chwieroth, A. Ginwalla, B.R. Patton, S.A. Akbar, P.K. Dutta, Composite n-p semiconducting titanium oxides as gas sensors, Sensors and Actuators B: Chemical 79 (2001) 17–27.

[39] J. Wang, P. Yang, X. Wei, High-performance, room-temperature, and no-humidity-impact ammonia sensor based on heterogeneous nickel oxide and zinc oxide nanocrystals, ACS Applied Materials & Interfaces 7 (2015) 3816–3824.
[40] H.-J. Kim, H.-M. Jeong, T.-H. Kim, J.-H. Chung, Y.C. Kang, J.-H. Lee, Enhanced ethanol sensing characteristics of In_2O_3-decorated NiO hollow nanostructures via modulation of hole accumulation layers, ACS Applied Materials & Interfaces 6 (2014) 18197–18204.
[41] G.S. Devi, S. Manorama, V.J. Rao, Gas sensitivity of SnO_2/CuO heterocontacts, Journal of the Electrochemical Society 142 (1995) 2754–2757.
[42] A.J.T. Naik, I.P. Parkin, R. Binions, Gas sensing studies of a n-n heterojunction array based on WO_3 and ZnO composites, IEEE Sensors Journal 14 (2014) 3137–3147.
[43] C. Sun, G. Maduraiveeran, P. Dutta, Nitric oxide sensors using combination of p- and n-type semiconducting oxides and its application for detecting NO in human breath, Sensors and Actuators B: Chemical 186 (2013) 117–125.
[44] T. Robert, M. Bartel, G. Offergel, Characterization of oxygen species adsorbed on copper and nickel oxides by x-ray photoelectron spectroscopy, Surface Science 33 (1972) 123–130.
[45] Y.M. Lu, W.S. Hwang, J.S. Yang, Effects of substrate temperature on the resistivity of non-stoichiometric sputtered NiOx films, Surface & Coatings Technology 155 (2002) 231–235.
[46] R.J.O. Mossanek, I. Preda, M. Abbate, J. Rubio-Zuazo, G.R. Castro, A. Vollmer, A. Gutiérrez, L. Soriano, Investigation of surface and non-local screening effects in the Ni 2p core level photoemission spectra of NiO, Chemical Physics Letters 501 (2011) 437–441.
[47] M.A. Peck, M.A. Langell, Comparison of Nanoscaled and Bulk NiO Structural and Environmental Characteristics by XRD, XAFS, and XPS, Chemistry of Materials 24 (2012) 4483–4490.
[48] J.C.C. Fan, J.B. Goodenough, X-ray photoemission spectroscopy studies of Sn-doped indium-oxide films, Journal of Applied Physics 48 (1977) 3524.
[49] S.T. Jun, G.M. Choi, Co gas-sensing properties of ZnO/CuO contact ceramics, Sensors and Actuators B: Chemical 17 (1994) 175–178.
[50] T. Taşköprü, M. Zor, E. Turan, Structural characterization of nickel oxide/hydroxide nanosheets produced by CBD technique, Materials Research Bulletin 70 (2015) 633–639.
[51] W.B. White, V.G. Keramida, Vibrational-spectra of oxides with c-type rare-earth oxide structure, Spectrochimica Acta Part A: Molecular Spectroscopy 28 (1972) 501.
[52] S.P. Mondal, P.K. Dutta, G.W. Hunter, B.J. Ward, D. Laskowski, R.A. Dweik, Development of high sensitivity potentiometric NOx sensor and its application to breath analysis, Sensors and Actuators B: Chemical 158 (2011) 292–298.
[53] N. Barsan, U. Weimar, Conduction model of metal oxide gas sensors, Journal of Electroceramics 7 (2001) 143–167.
[54] H.-J. Kim, J.-H. Lee, Highly sensitive and selective gas sensors using p-type oxide semiconductors: overview, Sensors and Actuators B: Chemical 192 (2014) 607–627.
[55] N. Barsan, C. Simion, T. Heine, S. Pokhrel, U. Weimar, Modeling of sensing and transduction for p-type semiconducting metal oxide based gas sensors, Journal of Electroceramics 25 (2010) 11–19.
[56] A. Gurlo, M. Sahm, A. Oprea, N. Barsan, U. Weimar, A p- to n-transition on α-Fe_2O_3-based thick film sensors studied by conductance and work function change measurements, Sensors and Actuators B: Chemical 102 (2004) 291–298.
[57] G. Korotcenkov, V. Brinzari, V. Golovanov, A. Cerneavschi, V. Matolin, A. Tadd, Acceptor-like behavior of reducing gases on the surface of n-type In_2O_3, Applied Surface Science 227 (2004) 122–131.
[58] N. Barsan, R. Grigorovici, R. Ionescu, M. Motronea, A. Vancu, Mechanism of gas-detection in polycrystalline thick-film SnO_2 sensors, Thin Solid Films 171 (1989) 53–63.
[59] T. Siciliano, A. Tepore, G. Micocci, A. Genga, M. Siciliano, E. Filippo, Transition from n- to p-type electrical conductivity induced by ethanol adsorption on α-tellurium dioxide nanowires, Sensors and Actuators B: Chemical 138 (2009) 207–213.
[60] A. Gurlo, N. Barsan, A. Oprea, M. Sahm, T. Sahm, U. Weimar, An n- to p-type conductivity transition induced by oxygen adsorption on alpha-Fe_2O_3, Applied Physics Letters 85 (2004) 2280–2282.
[61] X. Li, R. Ramasamy, P.K. Dutta, Study of the resistance behavior of anatase and rutile thick films towards carbon monoxide and oxygen at high temperatures and possibilities for sensing applications, Sensors and Actuators B: Chemical 143 (2009) 308–315.
[62] Y. Takao, K. Miyazaki, Y. Shimizu, M. Egashira, High ammonia sensitive semiconductor gas sensors with double-layer structure and interface electrodes, Journal of the Electrochemical Society 141 (1994) 1028–1034.
[63] I. Jimenez, M.A. Centeno, R. Scotti, F. Morazzoni, A. Cornet, J.R. Morante, NH_3 interaction with catalytically modified nano-WO_3 powders for gas sensing applications, Journal of the Electrochemical Society 150 (2003) H72–H80.
[64] I. Jimenez, M.A. Centeno, R. Scotti, F. Morazzoni, J. Arbiol, A. Cornet, J.R. Morante, NH_3 interaction with chromium-doped WO_3 nanocrystalline powders for gas sensing applications, Journal of Materials Chemistry 14 (2004) 2412–2420.
[65] C.P. Goyal, N.S. Ramgir, P.K. Sharma, N. Datta, M. Kaur, V. Parey, A.K. Debnath, F.Z. Haque, D.K. Aswal, S.K. Gupta, IEEE, NH_3 Sensing Characteristics of Pure and Al Modified WO_3 Thin Films, in: Proceedings of the "International Conference on Advanced Nanomaterials & Emerging Engineering Technologies" (ICANMEET-2013) organized by Sathyabama University, Chennai, India in association with DRDO, New Delhi, India, 2013, pp. 560–562, http://dx.doi.org/10.1109/ICANMEET. 2013.6609364.
[66] Y. Shimizu, T. Okamoto, Y. Takao, M. Egashira, Desorption behavior of ammonia from TiO_2-based specimens – ammonia sensing mechanism of double-layer sensors with TiO_2-based catalyst layers, Journal of Molecular Catalysis a-Chemical 155 (2000) 183–191.
[67] L. Wang, J. Pfeifer, C. Balazsi, I.M. Szildgyi, P.I. Gouma, in: Nanostructured hexagonal tungsten oxides for ammonia sensing, Proc. of SPIE 6769 (2007), 67690E-1–67690E-8. http://dx.doi.org/10.1117/12.736679.
[68] C.S. Rout, M. Hegde, A. Govindaraj, C.N. Rrao, Ammonia sensors based on metal oxide nanostructures, Nanotechnology 18 (2007) 205504.
[69] Y.-S. Kim, I.-S. Hwang, S.-J. Kim, C.-Y. Lee, J.-H. Lee, CuO nanowire gas sensors for air quality control in automotive cabin, Sensors and Actuators B: Chemical 135 (2008) 298–303.
[70] M. Che, A.J. Tench, Characterization and reactivity of molecular-oxygen species on oxide surfaces, Advances in Catalysis 32 (1983) 1–148.
[71] F. Almashta, N. Sheppard, V. Lorenzelli, G. Busca, Infrared study of adsorption on oxygen-covered alpha-Fe_2O_3 – bands due to adsorbed oxygen and their modification by CO-adsorbed hydrogen or water, Journal of the Chemical Society-Faraday Transactions I 78 (1982) 979–989.
[72] M. Courtois, S.J. Teichner, Infrared studies of CO, O_2, and CO_2 gases and their interaction products, chemically adsorbed on nickel oxide, Journal of Catalysis 1 (1962) 121–135.
[73] A.R. Gonzalezelipe, J.P. Holgado, R. Alvarez, G. Munuera, Use of factor-analysis and XPS to study defective nickel-oxide, Journal of Physical Chemistry 96 (1992) 3080–3086.
[74] Y. Zhang, P. Xu, J. Xu, H. Li, W. Ma, NH_3 sensing mechanism investigation of CuBr: different complex interactions of the Cu+ ion with NH_3 and O_2 molecules, Journal of Physical Chemistry C 115 (2011) 2014–2019.
[75] M.W. Roberts, Chemisorption and reaction pathways at metal surfaces: the role of surface oxygen, Chemical Society Reviews 18 (1989) 451–475.
[76] G.U. Kulkarni, C.N.R. Rao, M.W. Roberts, Nature of the oxygen species at Ni(110) and Ni(100) surfaces revealed by exposure to oxygen and oxygen-ammonia mixtures – evidence for the surface reactivity of O-type species, Journal of Physical Chemistry 99 (1995) 3310–3316.
[77] B. Lescop, A. Galtayries, G. Fanjoux, Thermal chemistry of NH_3 on oxygen-pretreated Ni(111) studied by metastable induced electron spectroscopy and ultraviolet photoelectron spectroscopy, Journal of Physical Chemistry B 108 (2004) 13711–13718.
[78] A.A. Tsyganenko, D.V. Pozdnyakov, V.N. Filimonov, Infrared study of surface species arising from ammonia adsorption on oxide surfaces, Journal of Molecular Structure 29 (1975) 299–318.
[79] E.C. Mattson, K. Pande, M. Unger, S. Cui, G. Lu, M. Gajdardziska-Josifovska, M. Weinert, J. Chen, C.J. Hirschmugl, Exploring adsorption and reactivity of NH_3 on reduced graphene oxide, Journal of Physical Chemistry C 117 (2013) 10698–10707.
[80] L. Chambon, C. Maleysson, A. Pauly, J.P. Germain, V. Demarne, A. Grisel, Investigation, for NH_3 gas sensing applications, of the Nb_2O_5 semiconducting oxide in the presence of interferent species such as oxygen and humidity, Sensors and Actuators B: Chemical 45 (1997) 107–114.
[81] M. Huebner, C.E. Simion, A. Tomescu-Stanoiu, S. Pokhrel, N. Barsan, U. Weimar, Influence of humidity on CO sensing with p-type CuO thick film gas sensors, Sensors and Actuators B: Chemical 153 (2011) 347–353.
[82] J.P. Gisbert, J.M. Pajares, Review article: ^{13}C-urea breath test in the diagnosis of H. Pylori infection-a critical review, Alimentary Pharmacology & Therapeutics 20 (2004) 1001–1017.

Biographies

Chenhu Sun received his B.S. and M.S. degrees in chemistry from Hunan University, Changsha, China. He is currently working on his Ph.D. in analytical chemistry at The Ohio State University, focusing on the development of solid-state electrochemical gas sensors and zeolites membranes.

Prabir K. Dutta received his Ph.D. degree in chemistry from the Princeton University. After four years of industrial research at Exxon Research and Engineering Company, he joined The Ohio State University, where currently he is a Distinguished University Professor. His research interests are in the area of microporous materials, including their synthesis, structural analysis and as hosts for chemical and photochemical reactions and ceramic sensors.